PHYSICAL REVIEW B VOLUME 15, NUMBER 2 15 JANUARY 1977

Angle-resolved photoemission from Cu single crystals using Al $K\alpha$ radiation

G. Apai, J. Stöhr, R. S. Williams, P. S. Wehner, S. P. Kowalczyk, and D. A. Shirley
Materials and Molecular Research Division, Lawrence Berkeley Laboratory, and Department of Chemistry, University of California, Berkeley, California 94720
(Received 4 October 1976)

Angle-resolved photoemission energy distributions (PED's) were obtained from valence bands of Cu single crystals using Al $K\alpha$ ($\hbar\omega = 1486.6$ eV) radiation. A pronounced difference in the PED's was observed between electron emission in the [001] and [111] directions. The observed differences are attributed to the symmetry properties of the $3d$ initial-state wave functions and are well described by the initial density of states modulated by an angle-dependent transition matrix element. An analytical expression is derived for this matrix element for tight-binding d initial and plane-wave final states.

I. INTRODUCTION

Angle-resolved photoemission spectra in the x-ray regime (XPS) from the valence bands of[1,2] Au and[2] Ag single crystals have been reported previously. The interpretation of such spectra is in general a nontrivial problem since no final-state band-structure calculations exist at such high energies, thus precluding detailed calculations.[3] The question arises whether an approximate model can be found which allows the interpretation of angle-resolved photoemission spectra in the XPS regime.[1,2] In order to elucidate this problem further we have measured photoelectron energy distributions (PED's) from the valence bands of Cu single crystals along the [001] and [111] directions. Experimental details and results are presented in Sec. II. In Sec. III we discuss the theoretical model suggested by Baird *et al.*[1] and compare it to the model used by McFeely *et al.*[2] For this latter model which emphasizes matrix-element effects in x-ray photoemission, an analytical expression is presented for the transition matrix element for photoemission from tight-binding d bands[4] into plane-wave final states. This allows one to calculate angle-resolved photoemission spectra for any photoemission direction with respect to the crystalline axes by means of a linear-combination-of-atomic-orbitals band-structure calculation[4] carried out in $\frac{1}{48}$ of the Brillouin zone (BZ). In Sec. IV we discuss the results of such a calculation for photoemission along the [001] and [111] directions for Cu and compare it to the experimental results.

II. EXPERIMENTAL DETAILS AND RESULTS

Two single crystals of copper with (001) and (111) surface orientations, respectively, were polished to 1-μm smoothness and etched in nitric acid to remove the damage layer formed by polishing. The crystals were oriented to within $\pm 1°$ by the Laue back-reflection method. Photoemission spectra were recorded with a Hewlett-Packard 5950A electron spectrometer modified for ultra-high-vacuum operation using monochromatized Al $K\alpha$ radiation (1486.6 eV). After introduction of the two crystals the preparation chamber of the spectrometer was baked to achieve a base pressure of $\sim 5 \times 10^{-10}$ Torr. The crystal surfaces were then cleaned by argon-ion bombardment and annealed by heating with an electron gun to remove surface damage. Cleanliness of the surfaces was checked by monitoring the carbon and oxygen 1s peak intensities. The carbon and oxygen 1s peaks were undetectable. Spectra were recorded for electrons propagating along the [001] direction of the (111) crystal and along the [111] direction of the (001) crystal. The experimental geometry is shown in Fig. 1. In both cases the nominal electron take-off angle from the crystal face was 35.5°. We estimate an angular accuracy for positioning the samples of $\pm 2°$ with a spectrometer solid angle of acceptance of $\pm(4 \pm 1)°$.

Experimental PED's from the valence bands of Cu using Al $K\alpha$ photons are shown in Fig. 2(a). The first spectrum was obtained earlier from a polycrystalline Cu sample.[5] The other two spectra were recorded using the single-crystal samples. They correspond to electron propagation along the [111] and [001] directions, respectively. It should be noted that all spectra shown in Fig. 2(a) represent raw data, without any smoothing, deconvolution, or background subtraction. The experimental resolution for the spectra, estimated from the full width half-maximum of the Au $4f_{7/2}$ line, is 0.8 eV. The detailed shapes of the Cu[111] and Cu[001] PED's are compared in Fig. 2(b). It is apparent that a distinct change in spectral shape exists between the two angle resolved PED's. Before discussing the results obtained by a theoretical model calculation, let us briefly discuss the

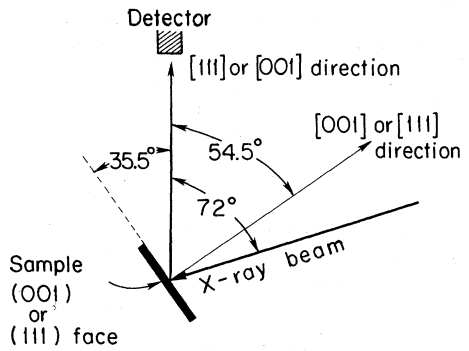

FIG. 1. Experimental geometry for angle-resolved photoemission studies at 1486.6 eV. The angle between the x-ray incidence and electron exit directions was fixed at 72°. Spectra were measured along the [111] direction of a crystal with a (001) surface orientation and along the [001] direction of a crystal with a (111) face.

basic features of the theoretical approximation employed here and also compare it to another model recently suggested by Baird *et al.*[1]

III. PHOTOEMISSION MODELS IN THE XPS REGIME

A. Direct-transition model

Baird *et al.* explained the angular variations of their photoemission spectra from Au valence bands in terms of a direct-transition model, which is illustrated in Fig. 3(b) for the case of photoemission into the [001] direction. Here we have assumed an angular resolution of ±4° and for simplicity have neglected the photon wave vector ($\vec{k}_{ph}=0$).[6] The basic assumption made by Baird *et al.* is that the magnitude of the photoelectron wave vector $\vec{q}$ inside the crystal is given by the *free-electron* dispersion relation $|\vec{q}|=(2mE_f/\hbar^2)^{1/2}$, where the final-state energy E_f is determined by the initial-state energy E_j and the photon energy $\hbar\omega$ ($E_f=E_j+\hbar\omega$). In this free-electron model the distribution of photoelectrons outside the crystal (wave vector $\vec{p}$) is determined by the crystal-vacuum boundary conditions $\vec{p}_{\parallel}=\vec{q}_{\parallel}$ and $p_{\perp}^2=q_{\perp}^2-2mV_0/\hbar^2$,[7] where $\vec{q}_{\parallel}$ and $q_{\perp}$ are the parallel and perpendicular components of $\vec{q}$ relative to the surface and V_0(≈14 eV for Cu) is the inner potential of the metal. At XPS energies $q_{\perp}^2 \gg 2mV_0/\hbar^2$ (except at low take-off angles) and the photoelectron angular distributions inside and outside the crystal are nearly the same. As seen from Fig. 3(b) the endpoints of all allowed $\vec{q}$ vectors then lie on a section of a sphere (in three dimensions) which may be approximated by a planar circular disk.[1,8] The location of the disk in the repeated zone scheme can be reflected back by an appropriate reciprocal lattice vector $\vec{G}$ into the first BZ, thus specifying the fraction of the first BZ (i.e., of all wave vectors $\vec{k}$ in the reduced zone scheme) which may contribute to photoemission into the analyzer.

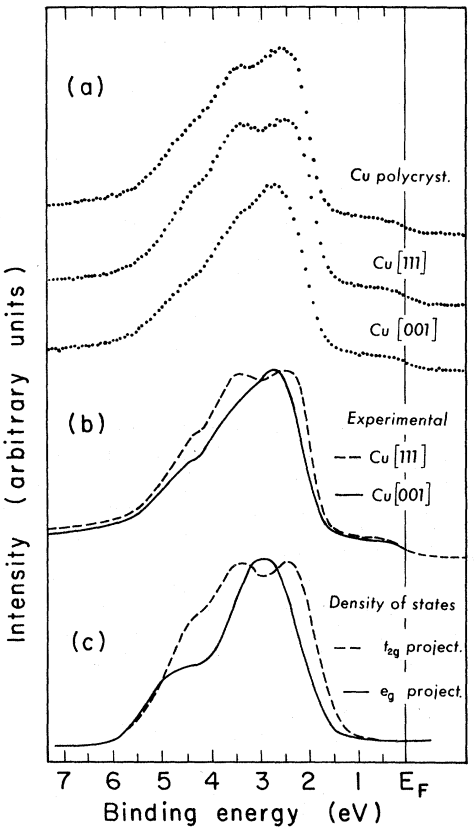

FIG. 2. (a) Experimental photoemission spectra from valence bands of Cu using Al $K\alpha$ radiation. The first spectrum was obtained with a polycrystalline (evaporated) Cu sample. The second spectrum was measured along the [111] direction, and the third spectrum along the [001] direction of a single crystal. (b) Comparison of the Cu[111] and Cu[001] spectra of Fig. 1(a). (c) Calculated t_{2g} and e_g projections of the total Cu 3*d* density of states using a tight-binding interpolation scheme as discussed in the text. The density-of-states histograms were convoluted with a Gaussian of full width at half-maximum of 0.8 eV.

Assuming constant-transition matrix elements the angle-resolved photoemission spectrum is then given by the density of states calculated over the so-determined $\vec{k}$ vectors and involving all bands which satisfy the detailed-energy conservation requirement $E_j(\vec{k})+\hbar\omega=E_f(\vec{k})$.[9] Variations in the PED's with angle in this model arise because different parts of the first BZ are sampled.

B. Matrix-element model

The present model was first discussed by McFeely *et al.*[2] in connection with angle-resolved PED's from Ag and Au valence bands. In contrast

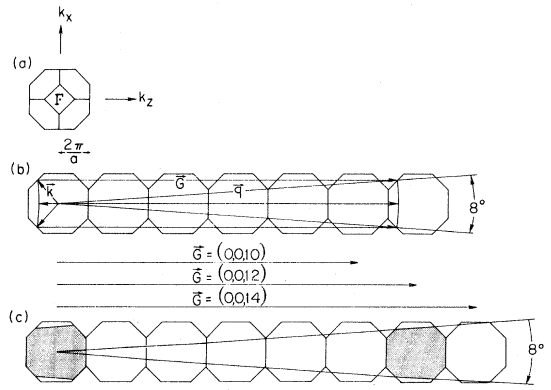

FIG. 3. (a) (010) projection of the three-dimensional Brillouin zone (BZ) of a fcc lattice with lattice constant a. The $\vec{k}$ axes are those of the infinite three-dimensional crystal. (b) Photoemission at $\hbar\omega = 1486.6$ eV along the [001] direction assuming an angular resolution of ±4° and free-electron final states. Only a small fraction of initial states in the first BZ (a cone of $\vec{k}$ vectors in three dimensions) can give rise to photoemission ($\vec{q}$ vectors) into the detector acceptance cone because of momentum conservation as discussed in the text. In the present example only final states which contain the reciprocal-lattice vector $\vec{G} = (0, 0, 12)$ contribute to photoemission. (c) Photoemission at $\hbar\omega = 1486.6$ eV along the [001] direction assuming an angular resolution of ±4° and Bloch-like final states. Because of mixing of the free-electron final states by the crystalline-potential initial states almost throughout the entire first BZ (dashed area) may contribute to photoemission to final Bloch states containing $\vec{G} = (0, 0, 12)$ components. The whole first BZ may contribute if the photon wave vector is taken into account as discussed in the text.

to Baird *et al.*, the latter authors pointed out that a more realistic description of the final states (i.e., Bloch sums rather than free-electron states) in conjunction with the finite acceptance angle of the analyzer, leads to sampling of *all* states in the first BZ. This point is illustrated in Fig. 3(c), again for photoemission in the [001] direction with an angular divergence of ±4° and $\vec{k}_{ph} = 0$ as an example. Because in a realistic band structure the final-state wave vector and energy are no longer related by the simple free-electron dispersion relation $E_f(\vec{k}) = \hbar^2|\vec{q}|^2/2m$ the magnitude of $\vec{q}$ inside the crystal is no longer fixed.[10] At $\hbar\omega = 1486.6$ eV, a great number of final Bloch states contain the reciprocal-lattice vector $\vec{G} = (0, 0, 12)$ and all such possible final states, which can enter the analyzer, are indicated as the shaded area in Fig. 3(c). When reflected back into the first BZ by $\vec{G} = (0, 0, -12)$ the shaded area indicates all initial states which may contribute to photoemission into the analyzer. Here it is important to state that even the small parts of the first BZ which cannot undergo transitions to final Bloch states containing $\vec{G} = (0, 0, 12)$ components may contribute if $\vec{G} = (0, 0, 14)$ components are considered or if the effect of the photon wave vector ($\vec{k}_{ph}$) is taken into account.[6] Because of the size of $\vec{k}_{ph}$ at $\hbar\omega = 1486.6$ eV,[6] the momentum conservation requirement $\vec{k}_{ph} + \vec{k} + \vec{G} = \vec{q}$ is not only satisfied by $\vec{G}$ vectors of the form $(0, 0, n)$ where n is an even integer,[11] but, depending on the direction of $\vec{k}_{ph}$, $\vec{G}$ vectors of the form $(\pm1, \pm1, 11)$, $(\pm1, \pm1, 13)$, $(\pm2, 0, 12)$, or $(0, \pm2, 12)$ may be involved. Thus, from a standpoint of *momentum* conservation, initial states within the whole first BZ may give rise to photoemission into a ±4° acceptance cone along the [001] direction, or in general along any given direction. However, in order for transitions to occur from a given initial state both *momentum* ($\vec{q} = \vec{k}_{ph} + \vec{k} + \vec{G}$) and *energy* [$E_f(\vec{k}) = E_i(\vec{k}) + \hbar\omega$] need to be conserved in the excitation process. In the XPS regime of photoemission the energy-conservation selection rule is relatively easily fulfilled at points throughout the first BZ because of the large number of final states present[12] and the mixing of these states by the crystal potential. This point is discussed in more detail by McFeely *et al.*[2]

In the above discussion we have assumed that the photoelectron angular distribution is the same inside and outside the crystal, i.e., we have neglected refraction of the photoelectrons at the crystal-vacuum interface. If the final Bloch state contains the reciprocal-lattice vector $\vec{G}$ a photoelectron with wave vector $\vec{k}_{ph} + \vec{k} + \vec{G} = \vec{q}$ is produced inside the crystal. The electron is then transmitted through the surface into a direction $\vec{p}$ outside the crystal, where $|\vec{p}|$ is related to the kinetic energy E_{kin} of the photoelectron according to $E_{kin} = \hbar^2|\vec{p}|^2/2m$. If α is the angle of incidence between $\vec{q}$ and the surface normal and β is the angle of refraction between $\vec{p}$ and the crystal normal, the boundary conditions are $\vec{p}_{\parallel} = \vec{q}_{\parallel}$ and $\sin\beta/\sin\alpha = |\vec{q}|/|\vec{p}|$.[13] The ratio $|\vec{q}|/|\vec{p}|$, which at XPS energies is essentially unity for free-electron final states, as discussed earlier, may deviate from 1 for Bloch-type final states because states throughout the first BZ are sampled causing $\vec{q} = \vec{k}_{ph} + \vec{k} + \vec{G}$ to deviate from the free-electron value. However, since at XPS energies $|\vec{G}| \gg |\vec{k}|$ the ratio $|\vec{q}|/|\vec{p}|$ is still approximately unity, refraction at the solid-vacuum interface may be neglected, except at low take-off angles. Under the above assumption that the whole first BZ contributes to photoemission and refraction at the surface is negligible, the angle-dependent PED's are thus given by the initial density of states where the various bands at each $\vec{k}$ point within the first BZ are weighted by an angle-dependent transition matrix element.[2]

As was shown in Ref. 2, the transition matrix element may conveniently be calculated by writing

the initial-state wave function in the tight-binding form[2,4] and assuming a plane-wave final state. Neglecting the s-part of the initial-state wave function, which only contributes a small and isotropic matrix element, one obtains the angle-dependent matrix element[2]

$$\sigma(\vec{k},j,\vec{q}) \sim \left| \sum_{\mu=1}^{5} \beta_\mu^j(\vec{k}) d_\mu(\theta_q,\phi_q) \right|^2 , \tag{1}$$

and the intensity distribution may be discussed in terms of the Fourier transforms of the d orbitals $d_\mu(\theta_r,\phi_r)$ listed in Table I. The coefficients $\beta_\mu^j(\vec{k})$ are obtained from a band-structure calculation.[4,14,15] Owing to our assumption that the whole first BZ is sampled, Eq. (1) may be further simplified by grouping the matrix elements of all equivalent points in the first BZ. The matrix elements of all equivalent points are obtained by transforming the d orbitals under the respective symmetry operations.[16] In this way it is seen that the various cross terms which occur in Eq. (1) cancel and one obtains the following analytical expression for the matrix element (compare Appendix A):

$$\sigma(\vec{k},j,\vec{q}) \sim 2(|\beta_1^j|^2 + |\beta_2^j|^2 + |\beta_3^j|^2)(d_1^2+d_2^2+d_3^2) + 3(|\beta_4^j|^2 + |\beta_5^j|^2)(d_4^2+d_5^2) . \tag{2}$$

Equation (2) demonstrates that the angle-dependent matrix element is in general a linear combination of the t_{2g} and e_g projections

$$\sigma_{t_{2g}}(\vec{k},j) \sim |\beta_1^j|^2 + |\beta_2^j|^2 + |\beta_3^j|^2 \tag{3}$$

and

$$\sigma_{e_g}(\vec{k},j) \sim |\beta_4^j|^2 + |\beta_5^j|^2 \tag{4}$$

of the initial-state tight-binding function. Because in deriving Eq. (2) we have transformed the wave function of all equivalent points in the first BZ into one irreducible wedge of the BZ, one may use Eq. (2) as weighting factors for a density-of-states calculation in the $\frac{1}{48}$ BZ. The angle-resolved photoemission spectrum in the XPS limit is then given by

$$N(E,\vec{q}) \sim \int_{1/48\ \mathrm{BZ}} d^3k \sum_j \sigma(\vec{k},j,\vec{q})\,\delta(E - E_j(\vec{k})) . \tag{5}$$

According to Eq. (2) photoemission along the [001] direction ($\theta_q = 0°$ and hence $d_1 = d_2 = d_3 = 0$) and along the [111] direction ($\theta_q = 54.7°$, $\phi_q = 45°$ and hence $d_4 = d_5 = 0$) represent the two extreme cases corresponding to the e_g and t_{2g} projections of the density of states.[17]

At this point we need to comment on previous calculations of the XPS photoemission spectra of *polycrystalline* d-band materials by Nemoshkalenko *et al.*[18] These authors claimed that by including angle averaged (integrated) matrix elements between tight-binding d initial states and plane-wave final states, they could account for part of the discrepancy between the experimental spectra and the calculated density of states. In particular they concluded that the electron excitation probability from e_g states is higher than from t_{2g} states. Our calculation, which employed the same description of initial and final states, is in gross disagreement with this result, since for polycrystalline materials, i.e., angle-integrated matrix elements, the e_g and t_{2g} states contribute equally to the photoemission spectrum. Equations (1) and (2) show that for this case the cross section (which is proportional to the transition probability) is given by

$$\sigma(\vec{k},j,\vec{q}) \sim \sum_m |\beta_m^j(\vec{k})|^2 . \tag{6}$$

This is exactly the *total* d projection of the initial states, i.e., the *sum* of the e_g and t_{2g} projections.[19] Only in case of angle-resolved photoemission from oriented single-crystal faces can the cross sections for photoemission from e_g and t_{2g} states be different.

TABLE I. Angular d orbitals.

	Label	Function	
d_1	d_{xy}	$(15/4\pi)^{1/2}\sin^2\theta\sin\phi\cos\phi$	t_{2g}
d_2	d_{yz}	$(15/4\pi)^{1/2}\sin\theta\cos\theta\sin\phi$	t_{2g}
d_3	d_{xz}	$(15/4\pi)^{1/2}\sin\theta\cos\theta\cos\phi$	t_{2g}
d_4	$d_{x^2-y^2}$	$\frac{1}{2}(15/4\pi)^{1/2}\sin^2\theta\cos2\phi$	e_g
d_5	$d_{3z^2-r^2}$	$(1/2\sqrt{3})(15/4\pi)^{1/2}(3\cos^2\theta-1)$	e_g

IV. DISCUSSION OF RESULTS

In Fig. 2(c) we show the results of a theoretical-model calculation employing Eq. (5) for photoemission into the [111] and [001] directions. As discussed earlier these cases correspond to the t_{2g} and e_g projections of the valence-band density of states. Comparison of Figs. 2(b) and 2(c) reveals good agreement between the experimental shapes of the PED's and the calculated ones. The main characteristic differences between the experimental spectra taken along the two symmetry directions are predicted well by the calculation. We note that plane-wave final-state cross section calculations should be more reliable for Cu than for the previously investigated noble metals Ag and Au.[2] This is inferred by the small-electron scattering phase shifts for Cu as opposed to the larger values for Ag and Au.[20] Also, the spin-orbit cou-

pling which reduces the $e_g - t_{2g}$ anistropy by mixing the wave functions is small for Cu. This might explain why the experimental and theoretical differences between the two directions are quite pronounced for Cu. It is interesting to note that our theoretical model predicts the largest changes to occur between the PED's taken along the [001] and [111] directions. This is in complete agreement with the experimental findings of Baird *et al.* for Au.[1] More evidence for the importance of matrix element effects in x-ray photoemission from *d* bands, as opposed to the constant matrix-element model proposed by Baird *et al.*, was recently presented by Williams *et al.*[21] These authors found good agreement between the angular variation of valence-band peak intensities of MoS_2 and that predicted by a tight-binding *d* initial- and plane-wave final-state matrix element. We feel that the present results, in conjunction with the results obtained earlier for Ag and Au,[2] indicate that the model presented above to explain the angular dependence of photoemission from *d* bands may, *in general*, provide a useful approximation in the x-ray range of photoemission.

APPENDIX A: TRANSFORMATION OF TIGHT-BINDING *d* FUNCTIONS IN A FIELD OF CUBIC SYMMETRY

Let $\psi_{\vec{k}}^{j}(\vec{r})$ be a tight-binding Bloch function

$$\psi_{\vec{k}}^{j}(\vec{r}) = N^{-1/2} \sum_{l} e^{i\vec{k}\cdot\vec{R}_l} \chi_j(\vec{r} - \vec{R}_l) , \tag{A1}$$

where $\chi_j(\vec{r} - \vec{R}_l)$ is a linear combination of atomic orbitals

$$\chi_j(\vec{r}) = \sum_{\mu} \beta_{\mu}^{j}(\vec{k}) \Phi_{\mu}(\vec{r}) . \tag{A2}$$

Let P be an operator, corresponding to one of the symmetry operations of the cubic group,[22] i.e., an operator which transforms a point $\vec{k}$ from one irreducible zone of the first BZ into an equivalent point in a different irreducible zone. Then the transformation of the corresponding Bloch function under P is given by[16]

$$P\psi_{\vec{k}}^{j}(\vec{r}) = \psi_{\vec{k}}^{j}(P^{-1}\vec{r}) = N^{-1/2} \sum_{n} e^{i\vec{k}\cdot\vec{R}_n} \chi_j(P^{-1}\vec{r} - \vec{R}_n) , \tag{A3}$$

where

$$\chi_j(P^{-1}\vec{r}) = \sum_{\mu} \beta_{\mu}^{j}(\vec{k}) \Phi_{\mu}(P^{-1}\vec{r}) . \tag{A4}$$

Thus the transformation of the tight-binding function $\psi_{\vec{k}}^{j}(\vec{r})$ is accomplished by simply transforming the atomic functions $\Phi_{\mu}(\vec{r})$ under the inverse operation P^{-1}. Furthermore, $\Phi_{\mu}(\vec{r})$ may be separated into a radial part $R(r)$ and an angular part $d_{\mu}(\theta_r, \phi_r)$. In the case of a simple fcc lattice the operations of the cubic group only affect the angular part, i.e., the *d* orbitals $d_{\mu}(\theta_r, \phi_r)$. Thus

$$\chi_j(P^{-1}\vec{r}) = R(r) \sum_{\mu} \beta_{\mu}^{j}(\vec{k}) P^{-1} d_{\mu}(\theta_r, \phi_r) . \tag{A5}$$

Knowing how the wave function $\psi_{\vec{k}}^{j}(\vec{r})$ transforms under P we can now transform its matrix element with a plane wave given by Eq. (1). Since this matrix element is the Fourier transform of the function

$$\sum_{\mu} \beta_{\mu}^{j}(\vec{k}) d_{\mu}(\theta_r, \phi_r) ,$$

we obtain

$$\left| \sum_{\mu} \beta_{\mu}^{j}(\vec{k}) P^{-1} d_{\mu}(\theta_q, \phi_q) \right|^2 \tag{A6}$$

for the transformed matrix element. Hence it is only necessary to work out the transformations of the five *d* orbitals under the 48 symmetry operations of the cubic group. This is easily done by writing the *d* orbitals in Cartesian coordinates. All t_{2g} orbitals (compare Table I) transform into each other (e.g., $P^{-1}d_2 = -d_3$) while the e_g orbitals either transform into themselves (i.e., $P^{-1}d_4 = d_4$ or $-d_4$ and $P^{-1}d_5 = d_5$) or into a linear combination of d_4 and d_5, i.e., $P^{-1}d_4 = \pm(\frac{1}{2}d_4 \pm \frac{1}{2}\sqrt{3}d_5)$ and $P^{-1}d_5 = \pm\frac{1}{2}\sqrt{3}d_4 - \frac{1}{2}d_5$. The sum of all 48 cross sections given by Eq. (A6), corresponding to the 48 equivalent *k* points in the first BZ then yields Eq. (2).

ACKNOWLEDGMENTS

We would like to thank Mrs. Winifred Heppler for preparation of the single crystals used in the present study and C. S. Fadley for communicating his angle resolved results for Cu prior to publication. Two of us (J.S. and P.S.W.) would like to acknowledge L. Falicov for an illuminating discussion. This work was done with support from the U. S. Energy Research and Development Administration.

[1] R. J. Baird, L. F. Wagner, and C. S. Fadley, Phys. Rev. Lett. 37, 111 (1976).
[2] F. R. McFeely, J. Stöhr, G. Apai, P. S. Wehner, and D. A. Shirley, Phys. Rev. B 14, 3273 (1976).
[3] See, for example, J. F. Janak, A. R. Williams, and V. L. Moruzzi, Phys. Rev. B 11, 1522 (1975).
[4] (a) L. Hodges, H. Ehrenreich, and N. D. Lang, Phys. Rev. 152, 505 (1966); (b) H. Ehrenreich and L. Hodges, in *Methods in Computational Physics*, edited by B. Alder, S. Fernbach, and M. Rotenberg (Academic,

New York, 1968), Vol. 8, p. 149.
[5]J. Stöhr, F. R. McFeely, G. Apai, P. S. Wehner, and D. A. Shirley, Phys. Rev. B 14, 4431 (1976).
[6]At $\hbar\omega = 1486.6$ eV $\vec{k}_{ph} = 0.43(2\pi/a)$, where a is the copper lattice constant (compare Fig. 3).
[7]G. D. Mahan, Phys. Rev. B 2, 4334 (1970).
[8]The thickness of the disk is determined by the width of the valence band (cf. Ref. 1).
[9]Note that the fraction of the first Brillouin zone which corresponds to the disk in the repeated zone scheme is determined by considering conservation of *momentum* only. Whether such states actually contribute depends on whether the detailed energy-conservation selection rule is satisfied at every $\vec{k}$ point. Baird *et al.* (Ref. 1) assume a free-electron final-state band structure for their detailed energy conservation.
[10]Note, however, that at XPS energies $|\vec{G}| \gg |\vec{k}|$ and the magnitude of $\vec{q} = \vec{k} + \vec{G}$ only needs to vary by a few percent to allow large fractions of the first BZ to be sampled.
[11]Only the components (0, 0, 10), (0, 0, 12), and (0, 0, 14) will be of importance, however, since the coefficients in the Bloch functions for $n < 10$ and $n > 14$ will decrease rapidly.
[12]The number of final states increases in good approximation as the square root of the photon energy.
[13]Compare the discussion on "secondary cones" in Ref. 7.
[14]N. V. Smith, Phys. Rev. B 3, 1862 (1971).
[15]Neglecting the small spin-orbit coupling for Cu, a 9 $\times$9 matrix was diagonalized at 308 points in the $\frac{1}{48}$ irreducible BZ (cf. Ref. 5) yielding the coefficients $\beta_\mu^j(\vec{k})$ where j is a band index and μ characterizes the contributions from the five d-orbital components.
[16]M. Tinkham, *Group Theory and Quantum Mechanics* (McGraw-Hill, New York, 1964), p. 279.
[17]Compare Eqs. (3-35) and (3-36) in Ref. 4b.
[18](a) V. V. Nemoshkalenko, V. G. Aleshin, Yu. N. Kucherenko, and L. M. Sheludchenko, Solid State Commun. 15, 1745 (1974); (b) V. V. Nemoshkalenko *et al.*, J. Electron. Spectrosc. Related Phenomena 6, 145 (1975); (c) V. V. Nemoshkalenko *et al.*, Phys. Scr. 11, 387 (1975); (d) V. V. Nemoshkalenko *et al.*, Solid State Commun. 16, 755 (1975).
[19]Note especially the discrepancy between our Eq. (6) and Eq. (6) in Ref. 18(c). This latter equation should read correctly

$$C^n_{t_{2g}}(\vec{k}) = [C^n_1(\vec{k})]^2 + [C^n_2(\vec{k})]^2 + [C^n_3(\vec{k})]^2$$

and

$$C^n_{e_g}(\vec{k}) = [C^n_4(\vec{k})]^2 + [C^n_5(\vec{k})]^2.$$

The error made by V. V. Nemoshkalenko *et al.* drastically affects their calculations and tends to make them look close to experiment by suppressing some of the t_{2g} intensity. This is seen from Fig. 4 of Ref. 18(c). It is apparent from this figure that a correct calculation including transition matrix elements (i.e., adding of e_g and t_{2g} projections in the lower spectrum in Fig. 4) only varies from the density of states insofar as the s part is suppressed.
[20]S. T. Manson, Phys. Rev. 182, 97 (1969).
[21]R. H. Williams, P. C. Kemeny, and L. Ley, Solid State Commun. 19, 495 (1976).
[22]See, for example, L. Pincherle, *Electronic Energy Bands in Solids* (McDonald, London, 1971).